Flash Flood Risk Assessment for Girne Region, Northern Cyprus

Youssef Kassem
Department of Mechanical Engineering
Engineering Faculty
Near East University
Nicosia, Cyprus
yousseuf.kassem@neu.edu.tr

Hüseyin Gökçekuş
Department of Civil Engineering
Civil and Environmental Engineering Faculty
Near East University
Nicosia, Cyprus
huseyin.gokcekus@neu.edu.tr

Nour Alijl
Department of Civil Engineering
Civil and Environmental Engineering Faculty
Near East University
Nicosia, Cyprus
nourshan2002@outlook.com

Received: 23 March 2022 | Revised: 12 April 2022 | Accepted: 30 April 2022

Abstract—Girne region is in the northern part of Northern Cyprus which is environmentally fragile and susceptible to natural disasters. Flash floods are a major problem in the region due to the heavy and torrential rainfalls in its urban environment. Therefore, this study aims to assess the flash flood risk for the Girne region, using the Geographic Information System (GIS). A mitigation flood risk plan is proposed and applied to the case study of the Girne region. The flood risk matrix is proposed based on the occurrence probability of the flood and the associated inundation depth. The risk matrix criterion was classified according to the degree of risks as high, moderate, and low. Five thematic maps affecting flood occurrences, including slope, elevation, land use, peak discharge, and flow accumulation, were classified to generate flood hazard maps. The results of the estimation of the magnitude of the inundation areas that can assess the degree of damage and its economic aspects are presented graphically. The developed flood risk matrix tool is a quantitative tool to assess damage and is essential for decision-makers.

Keywords- Flash flood, Girne, Northern Cyprus, GIS, flood risk matrix

I. INTRODUCTION

Floods may occur suddenly and be accompanied by other hazards such as landslides, mudflows, and damages to infrastructure [1, 2]. They occur due to the high intensity of rainfall within a shorter period [3]. The high-velocity runoff in small basins and the rapid rise of water and sediment transport have made flash floods extremely dangerous to infrastructure and human life. Flashfloods and used landslides have become major disasters worldwide [4]. In general, flash floods are the combined result of weather and geomorphological conditions [5-7]. Urban flooding is an essential issue globally due to its frequent occurrence that leads to damage to infrastructure and loss of lives. Flash floods in an urban area are recognized by the relatively short period of ephemeral water flow, which rarely lasts more than a day [8]. Thus, understanding the nature and the characteristics of flooding is one of the main goals of flood risk management. At present, flood maps are a potentially valuable tool for improving this understanding, but some drawbacks regarding the use of flood maps to mitigate flood risk and identify prone areas have been highlighted in the literature [9]. Anyhow, flood maps help to identify the most sensitive zones for civil protective actions, assess damages and make valid urban planning [8].

In Northern Cyprus, the coastal regions Girne (Kyrenia), Gazimağusa (Famagusta), and Güzelyurt (Morphou) are highly susceptible to urban flooding. During the recent years, heavy rain and thunderstorms affected over 3000 people, inflicting damages to the road network and the partial closure of a freeway in the Girne region [10-13]. This study aims to present a flood risk mitigation plan and a flood risk matrix technique for assessing risks in the urban Girne region of Northern Cyprus. The study focuses on the evaluation of the magnitude of the inundation areas and can assess the degree of damage from flash floods in the region for different frequencies of HEC-HMS hydrologic and 2D HEC-RAS hydraulic modeling techniques in order to delineate the inundation area at different degrees of flood hazards. To the best of our knowledge, there are no detailed studies in the Girne region regarding flash flood risk assessment.

II. MATERIALS AND METHODS

The proposed methodology aims to present a framework developed for flood modeling on regional scale combining GIS with a rainfall–runoff model (HEC-HMS) and a hydrologic

Corresponding author: Youssef Kassem

model (HEC-RAS). Figure 1 illustrates the methodology used in this study.

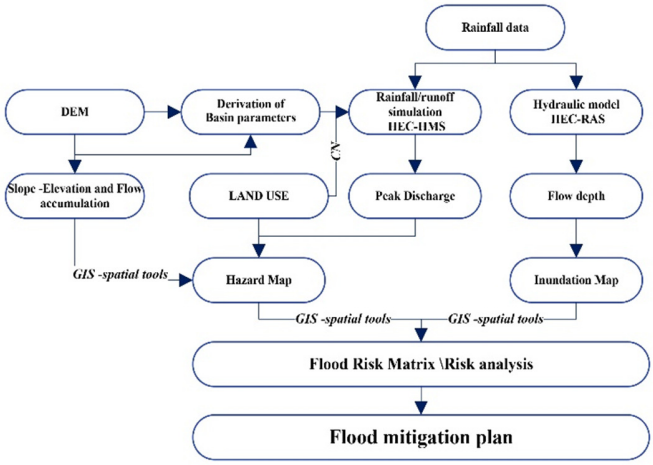

Fig. 1. The flowchart of the proposed methodology.

A. Study Area

Girne region is located in the northwest of Northern Cyprus at 35.2992° N latitude and 33.2363° E longitude as shown in Figure 2(a).

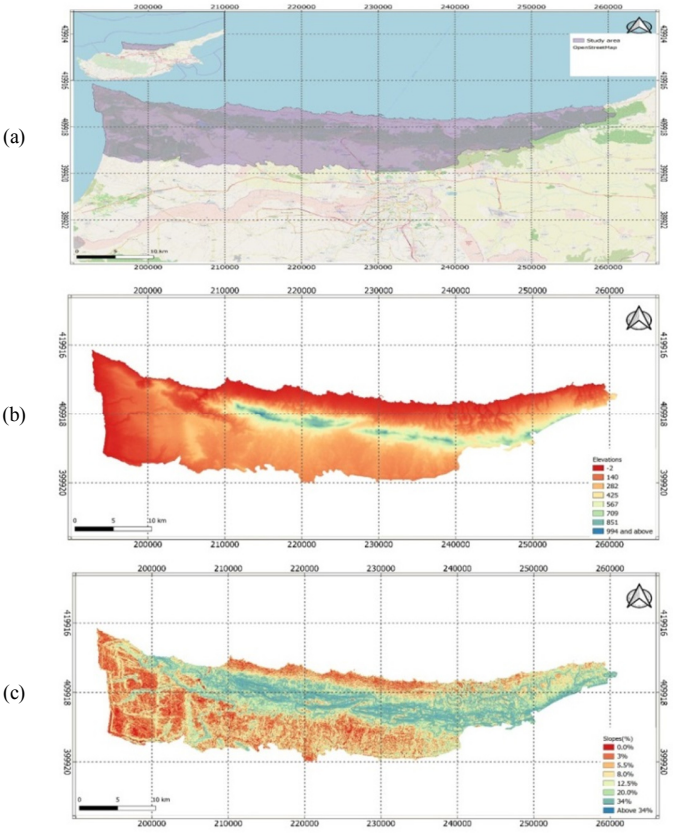

Fig. 2. The geographical location of Girne, Northern Cyprus: (a) Location, (b) elevation, (c) slopes.

It is surrounded by the Five Fingers mountain (Beşparmak), where elevations range from -2 to 1026m above sea level (Figure 2(b)), which has a major impact on defining the weather on the island. Slopes range from 0 % to 20% as shown in Figure 2(c). Rainfall distribution over the country varies considerably among regions. The minimum and maximum average values of rainfall in Mesaoria are 300 and 400mm whereas they are 400 and 450mm in the Karpas Peninsula area. Snow is rarely occurring on the upper hills of the Besparmak Mountains in the North and is usually present at the peaks of the Troodos Mountains in South Cyprus throughout the year. The maximum snowfall over the Northern part of Cyprus in the last ten years (1992-2002) was measured to be 15cm on Besparmak, Selvili Tepe, and Katara hills. Additionally, temperatures ranged from 21°C along the coast to 15°C on the top of the Girne. Maximum temperature can reach 45°C in the Mesaoria Plain. Moreover, there is no perennial stream in the Northern part of Cyprus. Twenty-eight streams located in the Northern part of Cyprus discharge about 27MCM of water annually [14]. Additionally, 10 ephemeral streams originating from the Troodos Mountain in the Southern part of Cyprus, discharge about 43MCM of water yearly [14]. Figure 3 shows the extracted channel networks and the flow connections from QGIS including dam locations.

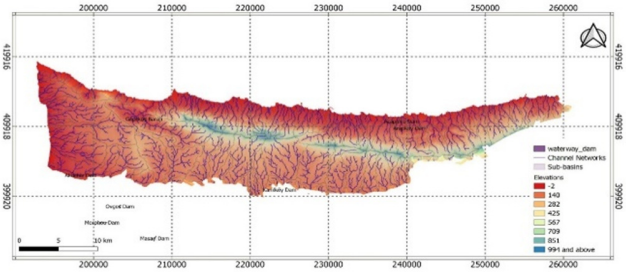

Fig. 3. Channel network and sub-basins-QGIS.

B. Extracted Digital Elevetion Model (DEM) and Hydrologic Analysis using QGIS and SAGA PLUG

Digital Elevation Model (DEM) data can be downloaded directly and are free for use from USGS earth explorer (https://earthexplorer.usgs.gov). The extracted 3D models of the earth's surface have cells that are represented as raster images in a pixel grid format. Each cell indicates the covered area's average elevation value. The model was improved by filling sinks and depressions locations with the Wang Liu algorithm. Catchments, Sub-Basins (SBs), flow accumulation, drainage sites, and flow directions will be used as input for runoff simulation after implementing spatial and hydrological analysis tools such as Quantum GIS (QGIS) and saga plug.

C. The Wang Liu Method

Virtually, all DEMs contain flat areas or depression pixels that may be actual landscape representations of artifacts. These features must be handled before any further hydrological analysis can be conducted [15]. Various algorithms have been developed for correcting these aspects, differing in how they handle the nature of the depressions. The Wang Liu method was utilized to fill sinks and depression areas in the extracted

DEM, and preserve the downward slope along the flow path, in addition, to enhancing hydrological analysis for surface elevations [15].

D. Rainfall Data and Return Period Analysis

The data have been collected from the Meteorological Department located in Lefkoşa, Northern Cyprus for a period from 1995 to 2015. Figure 4 shows the total amount of rainfall each year. The maximum and minimum values of total rainfall were recorded in 2012 and 2013 with a value of 593.86mm and 182.79mm respectively.

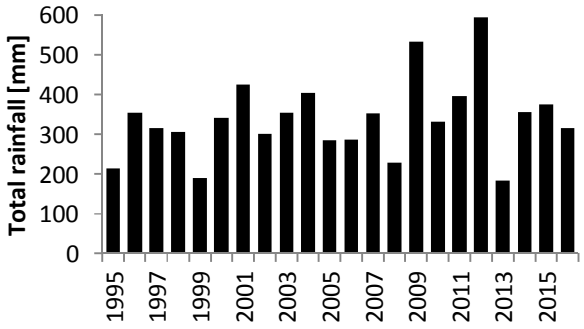

Fig. 4. Total amount of rainfall for the selected region.

Moreover, the estimation of the return period of high intensity of rainfall is particularly significant for many engineering elements including the construction of contour drains, dams, road culverts, airfield drainage, storm sewers in metropolitan areas, and flood or sediment control dams in water catchments. The measurement of the likely time interval between the occurrence of one event and the occurrence of a subsequent event of equal or larger magnitude is the return period. When a variable (X) equal to or higher than x occurs once every T years on average, then the probability of occurrence P is shown in (1) [16].

$$P = \frac{1}{T}(X \geq x) \quad or \quad T = \frac{1}{P}(X \geq x) \quad (1)$$

Several approaches have been presented to establish the plotting position, which refers to the probability value assigned to each piece of data to be plotted. Equation (2) is the most plotted position formula [16]:

$$P = \frac{1}{T} = \frac{m-b}{n+1-2b} \quad (2)$$

where m is the rank value in a list ordered by descending magnitude, n is the total number of values to be plotted, and b is a parameter that varies by formula (b=0.5 for Hazen, b=0.3 for Chegodayev, b=0 for Weibull, b=3/88 for Blom, b=1/3 for Tukey, and b = 0.44 for Gringoten) [16].

E. Assessment of Land Use, Soil Characteristics, and Curve Number (CN)

Surface runoff is the excessive rainfall after evaporation and infiltration have been excluded. Based on exhaustive rainfall/runoff data variety of land cover conditions and soil characteristics (moistures, structures, textures, and compactions), the method results in the establishment of a set of curves called Curve Number (CN). This empirical parameter is used in hydrology for predicting direct runoff or infiltration from rainfall excess. In general, soil groups are classified into four classes according to the Natural Resources Conservation Service (NRCS), which helps to identify land use classes and CN [17]. In this study, a virtual map (Figure 5) was prepared by utilizing spatial analysis tools in QGIS using Landsat-8 images, which were uploaded from USGS earth explorer dated on 20th of February 2020.

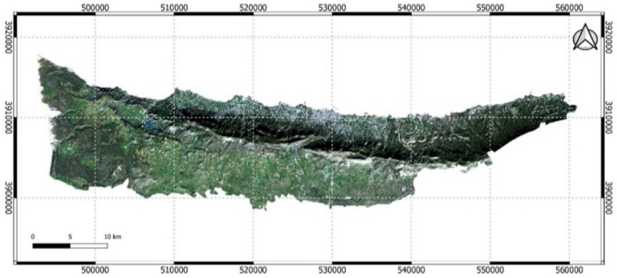

Fig. 5. Landsat-8 image -Girne /QGIS.

F. Rainfall-Runoff Simulation Model

Runoff simulation was done using HEC_HMS based on previous studies [18, 19] that utilized the software to assess flood impact and predict flows. The main elements to run simulation are: sub-basins, time-series data, control specifications, and metrological data. SCS CN was utilized to calculate the hydraulic loss rate. The 56 sub-basins were extracted using QGIS as shown in Figure 6.

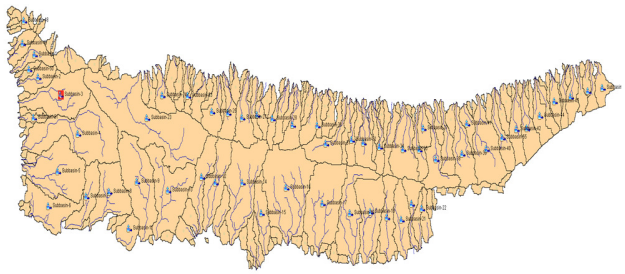

Fig. 6. Channel network and sub-basins-HEC-HMS.

G. Loss Method

Many methods have been utilized to simulate infiltration losses such as exponential, deficit and constant, initial and constant, Green and Ampt, Smith Parlange, and Soil Moisture Accounting– SMA SCS CN. The nominated method in this study is SCS CN which is used to determine the hydrologic loss rate. Equation (3) is used to calculate the runoff of the hydrographic basin:

$$Q = \frac{(P-0.2S)^2}{P+0.8S} \quad (3)$$

where Q is the surface runoff amount, P is the rainfall amount, and S is the potential maximum retention amount, which can be calculated by using the below function:

$$S = \left(\frac{25400}{CN}\right) - 254 \quad (4)$$

where *CN* is the curve number.

H. Transform Method

In previous studies, 7 methods have been employed to calculate the excess of precipitation to runoff: Mod-Clark, SCS unit hydrograph, user-specified graph, user-specified unit hydrograph), Snyder unit hydrograph, Clark unit hydrograph, and kinematic wave. The nominated method in this study was SCS unit hydrograph-based lag time calculated for each sub-basin. Lag time (*T*lag) represents the length of time between the peak discharges of the centroid of precipitation mass and the peak discharges of the resulting hydrograph it depends on the time of concentration (*TC*) as explained in (5) and the time of concentration (*TC*) calculated by (6) [20]:

$$T\text{lag} = 0.6\,TC \quad (5)$$

$$TC = \frac{4+\sqrt{H}+1.5L}{0.8\sqrt{H}} \quad (6)$$

where *L* represents the length of the main channel in km, *H* represents the difference between the mean basin elevation and the outlet elevation in m.

I. Weighting of Parameters Which Influence Flood Events

Based on the literature review and the Delphi approach [21, 22], 5 parameters were considered and rated to assess flood risk: Flow accumulation (F), Peak discharge (P), Elevation (E), Land use (L), and Slope (using ArcGIS). Spatial tool analysis was utilized to develop numerical thematic maps for flood hazard maps that were georeferenced to EPSG Projection 6312 Cyprus coordinate system. Parameter rating was done by applying Jenk's Natural Breaks method. The selected method classified Risk Levels (RLs) to 5 categories and assigned numerical values from 1 to 5: catastrophic RL = 5, severe RL = 4, major RL = 3, minor RL = 2, low RL = 1. Considering that the nominated parameters have different influences on flood generation. Correlation analysis was applied taking into consideration the influence of each factor on the other factors. Thus, two kinds of influence were utilized: major influence was assigned 1 point for the parameter bearing a direct influence on the remaining parameters, minor influence was assigned 1/2 point for first parameter bearing an indirect influence on the other parameters. The calculated rate is summarized in Table I.

TABLE I. INTERACTION BETWEEN FACTORS THAT INFLUENCE FLOOD RISK (FACTOR RATES)

Factor changing	Major effect	Minor effect	Factor rate
Flow accumulation (F)	(L)	(S)	1.5 points (1major + 1minor)
Slope (S)	(F), (L)		2.0 points (2major + 0minor)
Land use (L)	(F), (P)	(S)	2.5 points (2major + 1minor)
Peak discharge (P)	(F), (E)	(L)	2.5 points (2major + 1minor)
Elevation (E)	(R), (L), (F)	(S)	3.5 points (3major + 1minor)

III. RESULTS AND DISCUSSION

Based on the extracted factors, hazard and inundation prone areas with a high risk of flooding can be identified and to be used for risk matrix identification and quantitative analysis. Five thematic maps were developed and classified based on the selected method.

A. Catchment Area and Flow Delineation

The catchment consists of 56 sub-catchments with a total area of about 640km^2. The geometric and morphological parameters of the sub-catchment were used as main inputs to simulate runoff by utilizing the HEC-HMS model to calculate an excess of precipitation and peak discharge. Also, by utilizing the SCS method, *TC* and *T*lag were calculated. As shown in Figure 7, the highest values for *TC*, and *T*lag were found to be 229.39min and 137.64min respectively for sub-basin 10 and the minimum values were recorded for sub-basin 25 with a value of 48.25min and 28.90min respectively. This variation occurred due to the variance of elevation difference, stream length, and other morphological parameters influencing the estimation of the time of concentration.

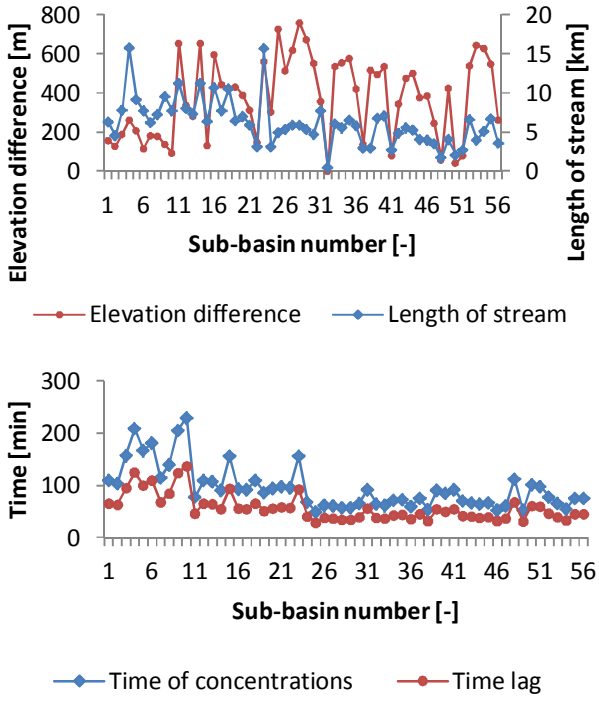

Fig. 7. Calculated values for time lag and time of concentrations.

B. Land Use - Land Cover and Curve Number Estimation

Remote sensing techniques were employed to classify Land Use and Land Cover (LULC). Girne LULC was extracted from the high-resolution Landsat-8 rasters, by utilizing spatial tool analysis in ArcGIS and maximum likelihood classifications based on NVDI. Five categories (road, woods, urban areas, vegetation, and pasture) were employed to calculate the CN in Figure 8. The maximum value of CN was 86.64 for sub-basin 1 which consists of 85% pasture area and the minimum value

was 82.52 for sub-basin 35 which consists of 65% wood area and 30% building area.

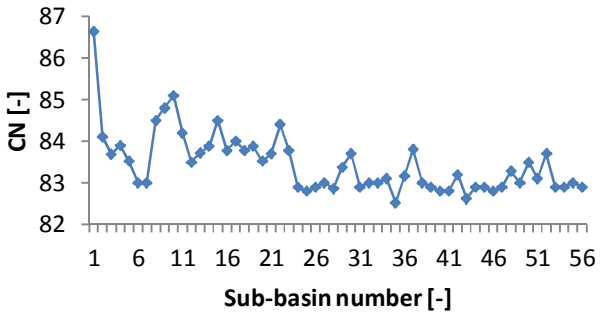

Fig. 8. Computed composite SCS-CN for the sub-basins.

C. Return Period Analysis

Six different methods were employed to calculate the design period for the annual maximum rainfall for the Girne region. As a result, the return design period of infrastructure hydraulic design is less than or equal to the recorded period data. The estimation of quintiles using empirical distribution functions or plotting point methods was followed. The return period of the 40.14mm event was 23 and 44 years, based on plotting points applied by the Hazen and Weibull methods respectively. The rainfall depth is estimated and summarized in Table II.

TABLE II. DESIGN RAINFALL FOR THE STUDY AREA

Design period	5 Years	10 Years	25 Years	50 Years	100 Years	200 Years
Rainfall	32.46	39.03	47.71	54.28	60.85	67.41

D. Rainfall-Runoff Simulation

In this study, the selected region is within ungagged catchments, and no runoff records were available. A Synthetic Unit Hydrograph (SUH) was utilized to calculate direct runoff and excess rainfall by using HEC-HMS. The main parameters in the utilized model are hydrological data and sub-catchment physical features. Computed runoff characteristics in terms of Peak Discharge (PD) value and Runoff Volume (RV) are summarized in Table III for various design periods. For example, it is found that the maximum value of PD was 15.3cu.m/s for sub-basin 23 with a total area of 41.40km^2, while the maximum RV was recorded for sub-basin 1 with a value of 381.68mm^3 for the selected design period with 2001 as the base year. It should be noted that the output from the model would be used as input for the hydraulic model.

E. Parameter Weighting and Map Classifications

Table IV lists the classification of the nominated factors into hazard levels. The calculated percentage of each parameter was found by multiplying the proposed weight of effect with the rate. In general, the hazardous area cannot be estimated by considering the effect of each factor independently. The integration of all factors is necessary to obtain the overall map of flood-hazard areas. Since not all factors have the same degree of influence on the hazardous areas, the weighting approach was applied. The selected parameters have the most substantial impact on flood risk based on their rate and weight, taking into consideration the cross-pollination between parameters. In this study, the ratings for the hazard levels (expert judgment), in points, which are illustrated in Table IV are: Catastrophic = 5, Major =4, Moderate = 3, Minor = 2, Low = 1. It should be noted these observations are supported by previous works [23, 24]. Moreover, the thematic maps were generated by utilizing GIS tools as shown in Figures 9 and 10. In this study, the high-risk areas are shown in blue colors such as Akdeniz, Grine, karakum, Geçitköy, Cape Kormakitis, and Karaoğlanoğlu with slopes less than 3.6% and elevations less than 129m. While the slope and higher elevation had minimal impact on the flood risk, the low-risk areas were shown in red color for the Five Fingers mountain (Beşparmak).

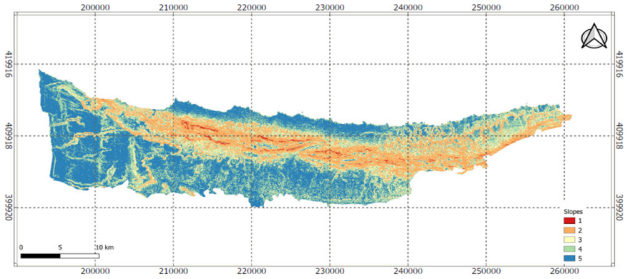

Fig. 9. Slope thematic map classification.

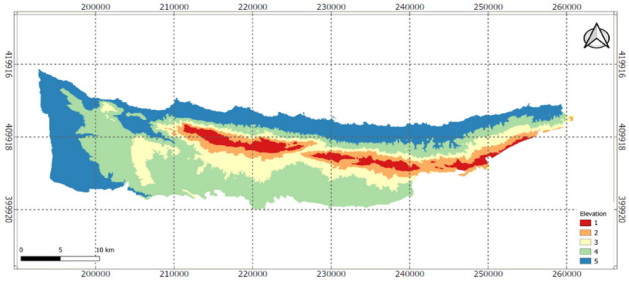

Fig. 10. Elevation thematic map classification.

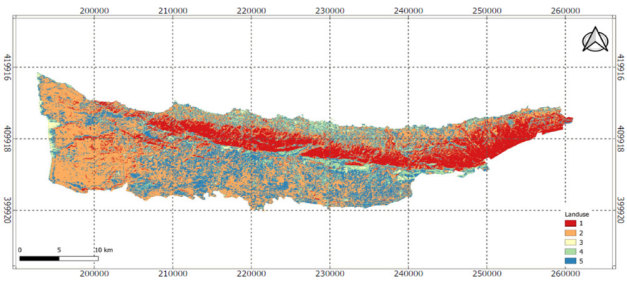

Fig. 11. Land use thematic map classification.

Additionally, a land-use/land cover map was extracted from the land sat-8 image. Land-use/land cover factor which influences the flood risk impact where the vegetation cover exists will reduce flood impact by controlling surface runoff when reaching the soil, while without vegetation cover in an urban area it will increase the flood risk as shown in Figure 11. This outcome is in accordance with the results of [23].

Peak discharge values were determined by utilizing runoff simulations and a thematic map (Figure 11) was generated by utilizing IDW (Inverse Distance Weighting) tool in GIS. Finally, the flow accumulation thematic map was extracted as shown in Figure 12. It is observed that sub-basins 4 and 2 have higher risk levels (i.e. blue color represents the high value of flow accumulation).

TABLE III. PEAK DISCHARGE AND RUNNOFF VOLUME

SB number	Area [km]	Base year 2001		5 years		10 years		25 years		50 years		100 years		200 years	
		PD [cu.m/s]	RV [mm]	PD [cu.m/s]	RV [mm]	PD [cu.m/s]	RV [mm]	PD [cu.m/s]	RV [mm]	PD [cu.m/s]	RV [mm]	PD [cu.m/s]	RV [mm]	PD [cu.m/s]	RV [mm]
Sb1	4.89	1.80	381.68	1.50	374.07	1.80	380.58	2.10	389.20	2.40	395.72	2.70	402.24	3.00	408.77
Sb2	4.84	1.80	372.67	1.50	365.08	1.70	371.58	2.10	380.17	2.40	386.67	2.60	393.17	2.90	399.67
Sb3	15.85	5.90	371.15	4.80	363.57	5.70	370.06	6.90	378.65	7.70	385.14	8.60	391.64	9.50	398.14
Sb4	27.87	10.30	371.95	8.50	364.36	10.00	370.86	12.10	379.44	13.60	385.94	15.20	392.44	16.70	398.94
Sb5	20.74	7.70	370.57	6.30	363.00	7.50	369.49	9.00	378.07	10.10	384.56	11.30	391.06	12.40	397.55
Sb6	12.72	4.70	368.69	3.90	361.11	4.60	367.60	5.50	376.17	6.20	382.66	6.90	389.15	7.60	395.65
Sb7	7.90	2.90	368.69	2.40	361.11	2.80	367.60	3.40	376.17	3.80	382.66	4.30	389.15	4.70	395.65
Sb8	12.36	4.60	374.10	3.80	366.51	4.50	373.01	5.40	381.61	6.10	388.11	6.70	394.61	7.40	401.12
Sb9	19.27	7.10	375.17	5.90	367.58	7.00	374.08	8.40	382.68	9.40	389.19	10.50	395.69	11.60	402.20
Sb10	19.65	7.30	376.24	6.00	368.65	7.10	375.15	8.60	383.75	9.60	390.26	10.70	396.77	11.80	403.28
Sb11	5.78	2.10	373.03	1.80	365.44	2.10	371.94	2.50	380.53	2.80	387.03	3.10	393.53	3.50	400.03
Sb12	13.63	5.00	370.50	4.20	362.92	4.90	369.41	5.90	377.99	6.70	384.49	7.40	390.98	8.20	397.48
Sb13	10.42	3.90	371.30	3.20	363.72	3.80	370.21	4.50	378.79	5.10	385.29	5.70	391.79	6.20	398.29
Sb14	24.55	9.10	371.87	7.50	364.29	8.90	370.78	10.60	379.37	12.00	385.87	13.40	392.37	14.70	398.87
Sb15	12.60	4.70	374.10	3.90	366.51	4.60	373.01	5.50	381.61	6.20	388.11	6.90	394.61	7.60	401.12
Sb16	29.69	11.00	371.51	9.10	363.93	10.70	370.42	12.90	379.01	14.50	385.51	16.20	392.00	17.80	398.50
Sb17	22.76	8.40	372.31	7.00	364.72	8.20	371.22	9.90	379.80	11.10	386.30	12.40	392.80	13.70	399.31
Sb18	15.88	5.90	371.51	4.80	363.93	5.70	370.42	6.90	379.01	7.80	385.51	8.60	392.00	9.50	398.50
Sb19	13.95	5.20	371.87	4.30	364.29	5.00	370.78	6.00	379.37	6.80	385.87	7.60	392.37	8.40	398.87
Sb20	9.20	3.40	370.57	2.80	363.00	3.30	369.49	4.00	378.07	4.50	384.56	5.00	391.06	5.50	397.55
Sb21	7.55	2.80	371.22	2.30	363.64	2.70	370.14	3.30	378.72	3.70	385.22	4.10	391.71	4.50	398.21
Sb22	7.01	2.60	373.74	2.10	366.16	2.50	372.65	3.00	381.25	3.40	387.75	3.80	394.25	4.20	400.76
Sb23	41.41	15.30	371.51	12.60	363.93	14.90	370.42	17.90	379.01	20.20	385.51	22.50	392.00	24.80	398.50
Sb24	7.62	2.80	368.32	2.30	360.75	2.70	367.23	3.30	375.81	3.70	382.30	4.10	388.79	4.60	395.28
Sb25	6.14	2.30	367.96	1.90	360.39	2.20	366.87	2.70	375.44	3.00	381.93	3.30	388.42	3.70	394.91
Sb26	7.27	2.70	368.32	2.20	360.75	2.60	367.23	3.10	375.81	3.50	382.30	3.90	388.79	4.30	395.28
Sb27	8.14	3.00	368.69	2.50	361.11	2.90	367.60	3.50	376.17	4.00	382.66	4.40	389.15	4.90	395.65
Sb28	9.19	3.40	368.18	2.80	360.61	3.30	367.09	4.00	375.66	4.50	382.15	5.00	388.64	5.50	395.13
Sb29	8.67	3.20	370.07	2.60	362.49	3.10	368.98	3.80	377.56	4.20	384.05	4.70	390.55	5.20	397.04
Sb30	11.29	4.20	371.22	3.40	363.64	4.10	370.14	4.90	378.72	5.50	385.22	6.10	391.71	6.80	398.21
Sb31	8.44	3.10	368.32	2.60	360.75	3.00	367.23	3.60	375.81	4.10	382.30	4.60	388.79	5.00	395.28
Sb32	7.12	2.60	368.69	2.20	361.11	2.60	367.60	3.10	376.17	3.50	382.66	3.90	389.15	4.30	395.65
Sb33	6.10	2.20	368.69	1.90	361.11	2.20	367.60	2.60	376.17	3.00	382.66	3.30	389.15	3.60	395.65
Sb34	12.27	4.50	369.05	3.70	361.48	4.40	367.96	5.30	376.54	6.00	383.03	6.70	389.52	7.30	396.01
Sb35	11.60	4.30	366.94	3.50	359.37	4.20	365.85	5.00	374.42	5.60	380.90	6.30	387.39	6.90	393.87
Sb36	3.73	1.40	369.27	1.10	361.69	1.30	368.18	1.60	376.76	1.80	383.25	2.00	389.74	2.20	396.23
Sb37	3.30	1.20	371.59	1.00	364.00	1.20	370.50	1.40	379.08	1.60	385.58	1.80	392.08	2.00	398.58
Sb38	8.73	3.20	368.69	2.70	361.11	3.10	367.60	3.80	376.17	4.30	382.66	4.70	389.15	5.20	395.65
Sb39	17.28	6.40	368.32	5.30	360.75	6.20	367.23	7.50	375.81	8.40	382.30	9.40	388.79	10.30	395.28
Sb40	14.51	5.30	367.96	4.40	360.39	5.20	366.87	6.30	375.44	7.10	381.93	7.90	388.42	8.70	394.91
Sb41	2.83	1.00	367.96	0.90	360.39	1.00	366.87	1.20	375.44	1.40	381.93	1.50	388.42	1.70	394.91
Sb42	6.28	2.30	369.41	1.90	361.84	2.30	368.33	2.70	376.90	3.10	383.39	3.40	389.89	3.80	396.38
Sb43	7.48	2.80	367.30	2.30	359.73	2.70	366.21	3.20	374.78	3.60	381.27	4.10	387.75	4.50	394.24
Sb44	7.93	2.90	368.32	2.40	360.75	2.80	367.23	3.40	375.81	3.90	382.30	4.30	388.79	4.30	388.79
Sb45	7.66	2.80	368.32	2.30	360.75	2.80	367.23	3.30	375.81	3.70	382.30	4.20	388.79	4.60	395.28
Sb46	3.76	1.40	367.96	1.10	360.39	1.40	366.87	1.60	375.44	1.80	381.93	2.00	388.42	2.20	394.91
Sb47	3.53	1.30	368.32	1.10	360.75	1.30	367.23	1.50	375.81	1.70	382.30	1.90	388.79	2.10	395.28
Sb49	4.22	1.60	368.69	1.30	361.11	1.50	367.60	1.80	376.17	2.10	382.66	2.30	389.15	2.50	395.65
Sb50	1.91	0.70	370.50	0.60	362.92	0.70	369.41	0.80	377.99	0.90	384.49	1.00	390.98	1.10	397.48
Sb51	3.61	1.30	369.05	1.10	361.48	1.30	367.96	1.60	376.54	1.80	383.03	2.00	389.52	2.20	396.01
Sb52	4.71	1.70	371.22	1.40	363.64	1.70	370.14	2.00	378.72	2.30	385.22	2.60	391.71	2.80	398.21
Sb53	16.22	6.00	368.32	4.90	360.75	5.80	367.23	7.00	375.81	7.90	382.30	8.80	388.79	9.70	395.28
Sb54	7.11	2.60	368.32	2.20	360.75	2.60	367.23	3.10	375.81	3.50	382.30	3.90	388.79	4.20	395.28
Sb55	11.59	4.30	368.69	3.50	361.11	4.20	367.60	5.00	376.17	5.60	382.66	6.30	389.15	6.90	395.65
Sb56	7.35	2.70	368.32	2.20	360.75	2.60	367.23	3.20	375.81	3.60	382.30	4.00	388.79	4.40	395.28

TABLE IV. CATEGORIZATION—CALIBRATION AND WEIGHT EVALUATION OF THE FACTORS AFFECTING FLOOD RISK AREAS IN GIRNE

Factors	Domain of effect	Descriptive level (flood risk level)	Proposed weight of effect (RL)	Rate (FR)	Weighted rating (FR*RL)	Total weight	Percentage
Slope	0-7.5	Catastrophic	5	2.0	10	30.0	17%
	7.5-15.0	Sever	4		8		
	15.0-25.0	Major	3		6		
	25.0-93.0	Minor	2		4		
	93.0 and above	Low	1		2		
Elevation	-5.0 - 129	Catastrophic	5	3.5	17.5	52.5	29%
	129.0 - 251.0	Sever	4		14		
	251 - 398	Major	3		10.5		
	398 - 603	Minor	2		7		
	603 - 1020	Low	1		3.5		
Land use (L)	Urban & bare area	Catastrophic	5	2.5	12.5	37.5	20%
	Scrub, annual crops	Sever	4		10		
	Permanent crops	Major	3		7.5		
	Pastures	Minor	2		5		
	Forest-woods	Low	1		2.5		
Flow accumulation (F)	27875 - 52789	Catastrophic	5	1.5	7.5	22.5	13%
	14087 - 27875	Sever	4		6		
	5798 - 14087	Major	3		4.5		
	1525 - 5798	Minor	2		3		
	0 - 1525	Low	1		1.5		
Peak discharge (P)	8.8 - 15.30	Catastrophic	5	1.5	12.5	37.5	21%
	6.4 - 8.8	Sever	4		10		
	4.5 - 6.4	Major	3		7.5		
	3.0 - 4.5	Minor	2		5		
	0.7 - 3.0	Low	1		2.5		

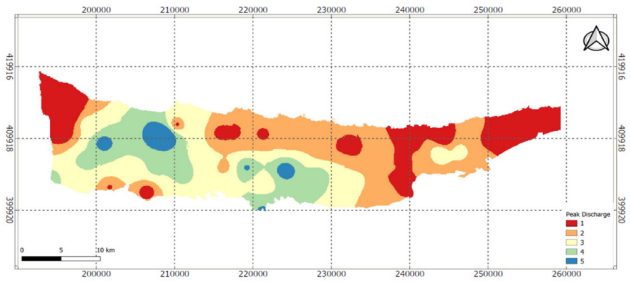

Fig. 12. Land use thematic map classification.

F. 2D Flood Mapping and Hydraulic Model using HEC-RAS

HEC-RAS was utilized to generate the hydraulic 2D flood mapping based on excessive precipitation and inflow hydrographs in unsteady flow conditions. The selected design periods were used to calculate Water Surface Elevation (WSE) and flow depth. For the next 5 years, the flood map predicts a maximum depth of 10.25m downstream and a minimum depth of 0.002m at high elevations, classifying the risk as catastrophic (the 25-year map is shown in Figure 13). A bit of water spreading over the mainstream and channel networks is shown while in the 50-year map more stream spreading were seen. For the 100- (Figure 14) and 200-year maps, the flood was significant and dominant. Other researchers who analyzed the inundation depth can support these observations. For instance, authors in [25] found that the flow depth for the low-risk area is less than 0.1m at the high elevation while 3m and above for high-risk areas mainly in major down streams.

Flood hazard maps, which were generated from the combined 5 thematics for different design periods were utilized to identify prone areas in the Girne region. In the context, lowlands, such as the Geçitköy located in the sub-basin 23 and Akdeniz in the sub-basin 4, are most vulnerable to flood occurrence, and meanwhile, at the highest land areas, minor risk occurs at Five Fingers mountain, while catastrophic risk areas in blue color are spreading in major downstream areas in Geçitköy. As illustrated in Figures 15 and 16, the low-risk area decreased from 30.42km^2 to 13.45km^2 while the catastrophic event area increased from 0.006km^2 to 4.344km^2. The differences are due to changes in land use, urban and human activities, and climate change.

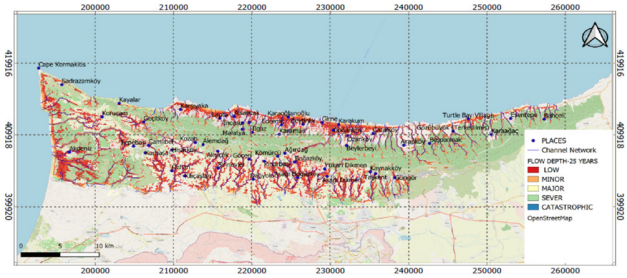

Fig. 13. 25 year design period flood inundation map.

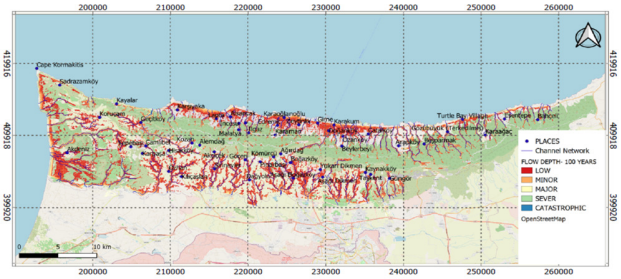

Fig. 14. 100 year design period flood inundation map.

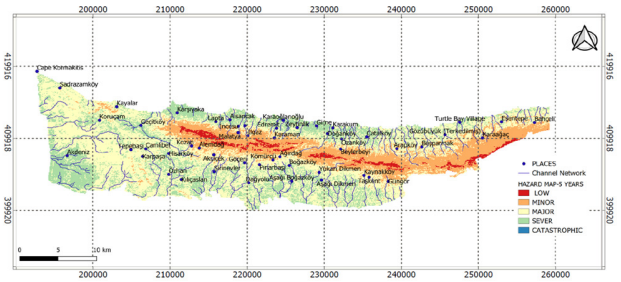

Fig. 15. Flash flood hazard map for the 25-year design period.

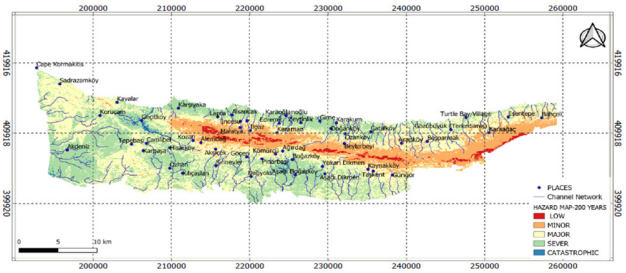

Fig. 16. Flash flood hazard map for the 100-year design period.

G. Risk Flood Matrix

The risk matrix (Figure 17) was established based on the likelihood of flow depth occurrence and its impact. A classified consequence (low, minor, major, severe, and catastrophic) is represented in a horizontal row, and the probability of occurrence of the return period in a vertical row. The degree of risk was determined by multiplying probability and impact, and the results were classified as low, medium, and high which are represented in green, yellow, and red, respectively.

Likelihood of Occurrence	Potential Consequences of flow depth				
	<0.10 m	0.10-0.50	0.50-1.00	1.00-2.00	>2
	1	2	3	4	5
	Low	Minor	Major	Sever	Catastrophic
Almost certain (every time)					
Likely (1-5 years)					
Possible (5-50 years)					
Unlikely (100 years)					
Rare (100-200 year)					

Legend: High, Medium, Low

Fig. 17. Flood risk matrix.

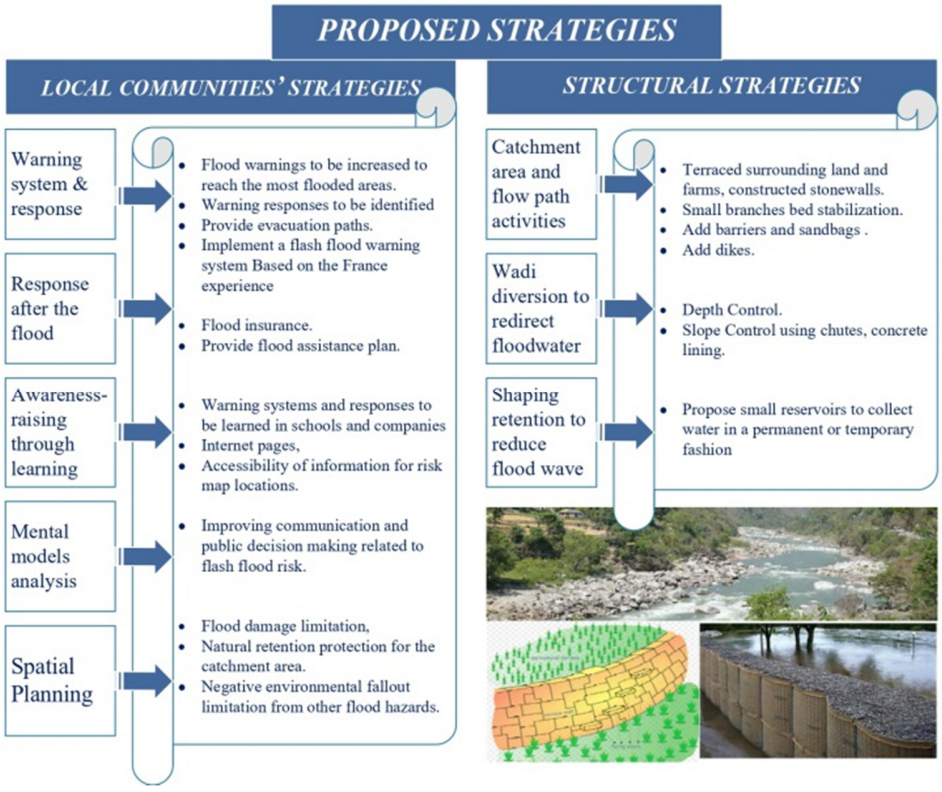

Fig. 18. Proposed strategies.

H. Defining Strategies

The strategies are classified into two categories, namely vulnerable local community and structural strategies [26-28]. The vulnerable local community strategy aims to eliminate and mitigate risk [27] due to the lack of response at an emergency. The structural strategy aims to control risk by reducing the impact of the flood. Figure 18 summarizes the classified straggles and examples for each category.

IV. CONCLUSIONS

The current paper intends to propose an established framework for a flood risk mitigation plan (Figure 19), which comprises data collected from weather forecasting in partnership with the water development department and crisis services. Hydrological analysis and risk analysis were conducted and measures were recommended. Flood parameters were illustrated in thematic maps in GIS using the IDW method. Peak discharge for various design periods was estimated using runoff simulation HEC-HMS. Flow depth was estimated using the hydrologic model HEC-RAS. Land uses were extracted from Landsat images-08. Elevation and slopes were extracted from a DEM. Flood hazard and inundation thematic maps revealed that lowlands are the most vulnerable to flooding, whereas higher land areas are less vulnerable to flood risk. The obtained results will assist planners and decision-makers in identifying prone areas to take appropriate and timely steps during the pre-disaster period.

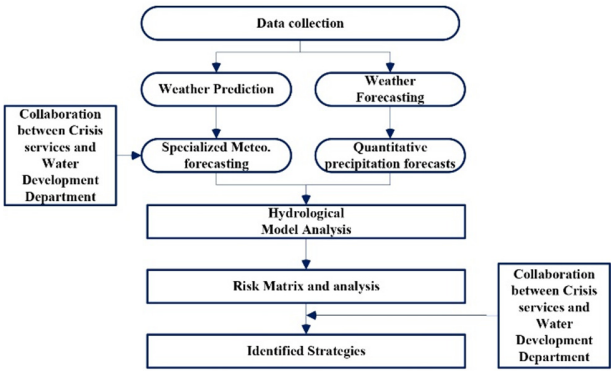

Fig. 19. Flood risk mitigation plan.

ACKNOWLEDGMENT

The authors would like to thank the Faculty of Engineering, especially the Mechanical Engineering Department at Near East University for their support and encouragement.

REFERENCES

[1] C. G. Collier, "Flash flood forecasting: What are the limits of predictability?," *Quarterly Journal of the Royal Meteorological Society*, vol. 133, no. 622, pp. 3–23, 2007, https://doi.org/10.1002/qj.29.

[2] A. A. Mahessar *et al.*, "Flash Flood Climatology in the Lower Region of Southern Sindh," *Engineering, Technology & Applied Science Research*, vol. 9, no. 4, pp. 4474–4479, Aug. 2019, https://doi.org/10.48084/etasr.2726.

[3] A. A. Sarker and A. K. M. M. Rashid, "Landslide and Flashflood in Bangladesh," in *Disaster Risk Reduction Approaches in Bangladesh*, R. Shaw, F. Mallick, and A. Islam, Eds. Tokyo, Japan: Springer Japan, 2013, pp. 165–189.

[4] M. Špitalar, J. J. Gourley, C. Lutoff, P.-E. Kirstetter, M. Brilly, and N. Carr, "Analysis of flash flood parameters and human impacts in the US from 2006 to 2012," *Journal of Hydrology*, vol. 519, pp. 863–870, Nov. 2014, https://doi.org/10.1016/j.jhydrol.2014.07.004.

[5] M. Abdel-Fattah, M. Saber, S. A. Kantoush, M. F. Khalil, T. Sumi, and A. M. Sefelnasr, "A Hydrological and Geomorphometric Approach to Understanding the Generation of Wadi Flash Floods," *Water*, vol. 9, no. 7, Jul. 2017, Art. no. 553, https://doi.org/10.3390/w9070553.

[6] S. Bisht, S. Chaudhry, S. Sharma, and S. Soni, "Assessment of flash flood vulnerability zonation through Geospatial technique in high altitude Himalayan watershed, Himachal Pradesh India," *Remote Sensing Applications: Society and Environment*, vol. 12, pp. 35–47, Nov. 2018, https://doi.org/10.1016/j.rsase.2018.09.001.

[7] P. K. Rai, R. S. Chandel, V. N. Mishra, and P. Singh, "Hydrological inferences through morphometric analysis of lower Kosi river basin of India for water resource management based on remote sensing data," *Applied Water Science*, vol. 8, no. 1, Jan. 2018, Art. no. 15, https://doi.org/10.1007/s13201-018-0660-7.

[8] T. L. Dammalage and N. T. Jayasinghe, "Land-Use Change and Its Impact on Urban Flooding: A Case Study on Colombo District Flood on May 2016," *Engineering, Technology & Applied Science Research*, vol. 9, no. 2, pp. 3887–3891, Apr. 2019, https://doi.org/10.48084/etasr.2578.

[9] P. Costabile, C. Costanzo, G. De Lorenzo, R. De Santis, N. Penna, and F. Macchione, "Terrestrial and airborne laser scanning and 2-D modelling for 3-D flood hazard maps in urban areas: new opportunities and perspectives," *Environmental Modelling & Software*, vol. 135, Jan. 2021, Art. no. 104889, https://doi.org/10.1016/j.envsoft.2020.104889.

[10] "Flood in Cyprus," *UN-SPIDER Knowledge Portal*. https://www.un-spider.org/advisory-support/emergency-support/3288/flood-cyprus.

[11] "Flooding Hits Kyrenia - Dam Overflows," *North Cyprus News*, Jan. 08, 2020. https://lgcnews.com/flooding-hits-kyrenia-dam-overflows/.

[12] "Heavy Rain Floods Kyrenia," *North Cyprus News*, Nov. 03, 2017. https://lgcnews.com/heavy-rain-floods-kyrenia/.

[13] "Cyprus – Flash Floods Leave 4 Dead," *FloodList*. https://floodlist.com/europe/cyprus-flash-floods-december-2018.

[14] Y. Kassem, H. Gökçekuş, and T. Rizza, "Groundwater Quality Assessment Based on Water Quality Index in Northern Cyprus," *Engineering, Technology & Applied Science Research*, vol. 12, no. 2, pp. 8435–8443, Apr. 2022, https://doi.org/10.48084/etasr.4790.

[15] Y. Liu, H. Liu, L. Wang, M. Xu, S. Cohen, and K. Liu, "Derivation of spatially detailed lentic habitat map and inventory at a basin scale by integrating multispectral Sentinel-2 satellite imagery and USGS Digital Elevation Models," *Journal of Hydrology*, vol. 603, Dec. 2021, Art. no. 126876, https://doi.org/10.1016/j.jhydrol.2021.126876.

[16] Y.-J. Wang, C.-Z. Qin, and A.-X. Zhu, "Review on algorithms of dealing with depressions in grid DEM," *Annals of GIS*, vol. 25, no. 2, pp. 83–97, Apr. 2019, https://doi.org/10.1080/19475683.2019.1604571.

[17] J. Yuan, K. Emura, C. Farnham, and M. A. Alam, "Frequency analysis of annual maximum hourly precipitation and determination of best fit probability distribution for regions in Japan," *Urban Climate*, vol. 24, pp. 276–286, Jun. 2018, https://doi.org/10.1016/j.uclim.2017.07.008.

[18] Natural Resources Conservation Service, *National Engineering Handbook Hydrology*. Washington DC, USA: United States Department of Agriculture, 2007.

[19] W. Gumindoga, D. T. Rwasoka, I. Nhapi, and T. Dube, "Ungauged runoff simulation in Upper Manyame Catchment, Zimbabwe: Application of the HEC-HMS model," *Physics and Chemistry of the Earth, Parts A/B/C*, vol. 100, pp. 371–382, Aug. 2017, https://doi.org/10.1016/j.pce.2016.05.002.

[20] W. A. Scharffenberg, "HEC-HMS User's Manual," US Army Corps of Engineers, HEC, Washington DC, USA, Dec. 2013.

[21] M. Giandotti, "Previsione delle piene e delle magre dei corsi d'acqua," 1933.

[22] J. Liu, Z. Xu, F. Chen, F. Chen, and L. Zhang, "Flood Hazard Mapping and Assessment on the Angkor World Heritage Site, Cambodia," *Remote Sensing*, vol. 11, no. 1, Jan. 2019, Art. no. 98, https://doi.org/10.3390/rs11010098.

[23] N. Kazakis, I. Kougias, and T. Patsialis, "Assessment of flood hazard areas at a regional scale using an index-based approach and Analytical Hierarchy Process: Application in Rhodope–Evros region, Greece," *Science of The Total Environment*, vol. 538, pp. 555–563, Dec. 2015, https://doi.org/10.1016/j.scitotenv.2015.08.055.

[24] N. N. Kourgialas and G. P. Karatzas, "Flood management and a GIS modelling method to assess flood-hazard areas—a case study," *Hydrological Sciences Journal*, vol. 56, no. 2, pp. 212–225, Mar. 2011, https://doi.org/10.1080/02626667.2011.555836.

[25] G. D. Bathrellos, H. D. Skilodimou, K. Soukis, and E. Koskeridou, "Temporal and Spatial Analysis of Flood Occurrences in the Drainage Basin of Pinios River (Thessaly, Central Greece)," *Land*, vol. 7, no. 3, Sep. 2018, Art. no. 106, https://doi.org/10.3390/land7030106.

[26] Y. Zhang, Y. Wang, Y. Chen, F. Liang, and H. Liu, "Assessment of future flash flood inundations in coastal regions under climate change scenarios—A case study of Hadahe River basin in northeastern China," *Science of The Total Environment*, vol. 693, Nov. 2019, Art. no. 133550, https://doi.org/10.1016/j.scitotenv.2019.07.356.

[27] C. Samela, R. Albano, A. Sole, and S. Manfreda, "A GIS tool for cost-effective delineation of flood-prone areas," *Computers, Environment and Urban Systems*, vol. 70, pp. 43–52, Jul. 2018, https://doi.org/10.1016/j.compenvurbsys.2018.01.013.

[28] "Guidance on Flash Flood Management Recent Experiences from Central and Eastern Europe," *CORE*, 2007. https://core.ac.uk/display/22563624.